Strong magneto-optical effects in ACr_2O_4 (A = Fe, Co) spinel oxides generated by tetrahedrally coordinated transition metal ions

V. Kocsis,[1,2] S. Bordács,[1] J. Deisenhofer,[3] L. F. Kiss,[4] K. Ohgushi,[5] Y. Kaneko,[2] Y. Tokura,[2,6] and I. Kézsmárki[1,3]

[1]*Department of Physics, Budapest University of Technology and Economics and MTA-BME Lendület Magneto-optical Spectroscopy Research Group, 1111 Budapest, Hungary*

[2]*RIKEN Center for Emergent Matter Science (CEMS), Wako, Saitama 351-0198, Japan*

[3]*Experimental Physics 5, Center for Electronic Correlations and Magnetism, Institute of Physics, University of Augsburg, 86159 Augsburg, Germany*

[4]*Institute for Solid State Physics and Optics, Wigner Research Centre for Physics, Hungarian Academy of Sciences, 1525 Budapest, Hungary*

[5]*Department of Physics, Graduate School of Science, Tohoku University, 6-3, Aramaki Aza-Aoba, Aoba-ku, Sendai, Miyagi 980-8578, Japan*

[6]*Department of Applied Physics, University of Tokyo, Hongo, Tokyo 113-8656, Japan*

(Received 30 November 2017; published 23 March 2018)

Magneto-optical effects have been investigated over the infrared visible spectral range in ACr_2O_4 (A = Fe,Co) spinel oxides with noncollinear spin orders in their ground states. We found large magneto-optical Kerr rotation and ellipticity at the on-site d-d transitions of the A^{2+} ions located within the charge gap. The magneto-optical Kerr rotation of $\vartheta_{\mathrm{Kerr}} \approx 12^\circ$ observed in $CoCr_2O_4$ is unprecedentedly large among magnetic semiconductors and points toward the uniqueness of tetrahedrally coordinated Co^{2+} ions in generating strong magneto-optical response. Criteria of strong magneto-optical effects emerging at on-site d-d transitions of transition metal ions are discussed.

DOI: 10.1103/PhysRevB.97.125140

I. INTRODUCTION

Optical rotators and isolators, produced from materials with a strong Faraday effect, such as CdMnTe and CdMnHgTe [1,2], are important building blocks of optical fiber networks. The Faraday effect, which is the polarization rotation of light traveling through a magnetic media, is induced by magnetocircular birefringence. The magneto-optical Kerr effect (MOKE), another manifestation of the magnetocircular birefringence and dichroism, is the polarization change upon the reflection of light from the surface of magnetic materials [3–6]. The MOKE provides a figure of merit for the magnetic control of light polarization due to the simplicity and small requirements toward the optical elements utilizing this phenomenon. In addition to applications, large magneto-optical effects can also be used as a sensitive probe to explore magnetic phase boundaries, as was demonstrated recently in the skyrmion-host insulator Cu_2OSeO_3 where a large Faraday effect was observed not only in the visible [7], but also in the THz spectral range [8].

The principal material parameters governing the magnitude of the magneto-optical effects are the spin polarization of the photoexcited states and the strength of the spin-orbit coupling (SOI) acting on these states. In itinerant magnets, the MOKE can be enhanced in the vicinity of the plasma resonance [9,10], reaching magneto-optical Kerr rotation as large as $\vartheta_{\mathrm{Kerr}} \approx 90^\circ$ found in CeSb [11,12]. In such cases, the large MOKE effects usually arise from moderate values of the off-diagonal conductivity, which are highly enhanced by the strong dispersion of the reflectivity in the plasma-edge region and the magnetic-field-induced shift of the plasma edge [9,10]. In insulating magnets, strong magneto-optical effects have been observed in resonance with on-site d-d or f-f optical excitations of magnetic ions [13–18]. Contrary to itinerant magnets, here the enhanced MOKE is mainly attributed to the strong spin-orbit coupling as the optical resonances are located in the optical gap. Recently, chromium spinel oxides and chalcogenides exhibiting large magnetocapacitance [19,20], magneto-optical [14,21], and magnetoelastic [10,22] effects have attracted much interest.

At room temperature, $FeCr_2O_4$ and $CoCr_2O_4$ have the normal cubic spinel structure belonging to the $Fd\bar{3}m$ space group [23–25]. The structural unit cell of ACr_2O_4 spinels contains two A^{2+} ions, which constitute a diamond sublattice with tetrahedral oxygen coordination, while the Cr^{3+} ions form a pyrochlore lattice. Due to the orbital degeneracy of Fe^{2+} ions in the cubic spinel structure, $FeCr_2O_4$ undergoes a cooperative Jahn-Teller distortion at $T_{\mathrm{JT}} = 135$ K [10,22,25,26], which reduces the crystal symmetry to tetragonal with the $I4_1/amd$ space group [25]. In contrast, in $CoCr_2O_4$ with no orbital degree of freedom, no measurable distortion of the cubic structure has been detected down to $T = 10$ K [10,22].

At low temperatures, both spinel oxides show noncollinear ferrimagnetic order [14]. According to neutron scattering measurements on $CoCr_2O_4$, the ferrimagnetic structure arising below $T_{\mathrm{C}} \approx 93$ K is followed by an incommensurate transverse conical spin reordering on both the Co and Cr sublattices at $T_{\mathrm{S}} = 26$ K, which becomes commensurate at $T_{\text{lock-in}} = 13$ K [27]. Below its ferrimagnetic ordering at $T_{\mathrm{C}} \approx 70$ K, $FeCr_2O_4$ was also reported to develop a conical spin order at $T_{\mathrm{S}} = 35$ K [28], although the details of this magnetic structure have not been investigated yet. In $FeCr_2O_4$, the ferrimagnetic transition is accompanied by further reduction of the symmetry to orthorhombic due to magnetoelastic effects [10,22,29].

In this work, we study the MOKE in $CoCr_2O_4$ and $FeCr_2O_4$ and report large magneto-optical Kerr rotation emerging at

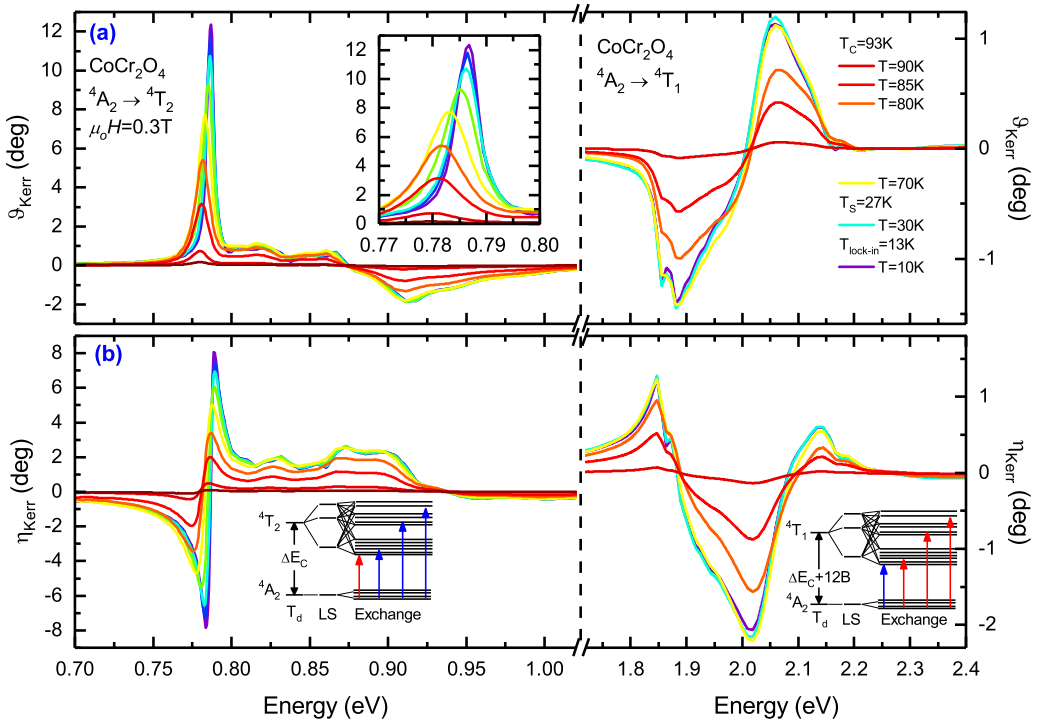

FIG. 1. Temperature dependence of the complex magneto-optical Kerr rotation spectra of $CoCr_2O_4$ over the near-infrared–visible region measured in $\mu_oH = 0.3$ T magnetic field. (a) [(b)] Magneto-optical Kerr rotation (ϑ_{Kerr}) [ellipticity (η_{Kerr})] spectra at the $^4A_2 \rightarrow {}^4T_2$ and $^4A_2 \rightarrow {}^4T_1$ transitions of the Co^{2+} ions. Note the breaks of the horizontal axes between the two transitions and the different vertical scales used at the two sides of the breaks. A huge peak is observed in the Kerr rotation spectrum at the low-energy side of the $^4A_2 \rightarrow {}^4T_2$ transition with a maximum of about 12° at $T = 10$ K. See the inset in panel (a) for an enlarged view of the peak in ϑ_{Kerr}. This peak is accompanied with a strong dispersive signal in the Kerr ellipticity. The splitting of the Co^{2+} $3d$ multiplets is schematically reproduced from Refs. [14,33] with the following hierarchy of the interactions: (i) crystal field of the O_4 tetrahedron surrounding the Co ion, (ii) spin-orbit interaction, and (iii) exchange interaction. Blue (red) arrows correspond to the $J_z \rightarrow J_z + 1$ ($J_z \rightarrow J_z - 1$) transitions excited by right (left) circularly polarized photons. J_z denotes the angular momentum of the $3d$ electrons along the quantization axis, i.e., the direction of the external magnetic field.

the on-site d-d transitions of the tetrahedrally coordinated magnetic A^{2+} ions. To the best of our knowledge, the magneto-optical Kerr rotation of $\vartheta_{Kerr} \approx 12°$ observed in $CoCr_2O_4$ for photon energies close to 0.78 eV (close to the 1.55 μm widely used in telecommunication) is the highest ever observed in magnetic semiconductors and insulators.

II. EXPERIMENTAL DETAILS

Single crystals of $CoCr_2O_4$ used in the present study were grown by the chemical vapor transport method as presented in Ref. [14]. $FeCr_2O_4$ single crystals were obtained by the floating zone technique. FeO and Cr_2O_3 were mixed and sintered in an argon atmosphere for 12 h at 1200 °C. Then after regrinding, the resultant was pressed into a rod shape and further heated in an Ar + 1%H_2 atmosphere for 12 h at 1300 °C. Single crystals of $FeCr_2O_4$ were formed in an Ar + 0.1%H_2 atmosphere at a pressure of 2 atm in a halogen-incandescent lamp floating zone furnace (SC-N35HD, NEC).

Temperature-dependent reflectivity spectra were measured, and a diagonal component of the optical conductivity was calculated via Kramers-Kronig transformation as reported in a previous study [22]. The complex Kerr rotation, Φ_{Kerr}, was measured at nearly normal incidence on the (001) surface of the crystals by a broadband dual-channel magneto-optical spectrometer as described in earlier papers [10,30,31]. Magnetic fields of $\mu_oH = \pm 0.3$ T were applied along the propagation vector of the incident light by permanent magnets ensuring the polar MOKE geometry. The off-diagonal component of the optical conductivity σ_{xy} was evaluated using the diagonal optical conductivity σ_{xx} and the complex Kerr rotation, i.e., the Kerr rotation ϑ_{Kerr} and the Kerr ellipticity η_{Kerr}, according to the relation [5,32]

$$\Phi_{Kerr} = \vartheta_{Kerr} + i\eta_{Kerr} = \frac{\sigma_{xy}}{\sigma_{xx}\sqrt{1 + \frac{i\sigma_{xx}}{\omega}}}. \quad (1)$$

Temperature-dependent magnetization was measured with a SQUID magnetometer (MPMS-5S, Quantum Design) in $\mu_oH = 0.3$ T, in accordance with the MOKE experiments.

III. RESULTS AND DISCUSSION

A. Magneto-optical Kerr rotation spectra

The temperature dependences of the complex Kerr rotation spectra of $CoCr_2O_4$ and $FeCr_2O_4$ in the near-infrared–visible region are, respectively, shown in Figs. 1 and 2. In the ferrimagnetic state of the materials, a strong MOKE is found in the energy range of the d-d excitations of the magnetic A^{2+} ions. The assignment and the fine structure of the transitions are reproduced from Refs. [14,33] in the inset of the figures. In the ferrimagnetic phase, strong and sharp peaks emerge in the Kerr

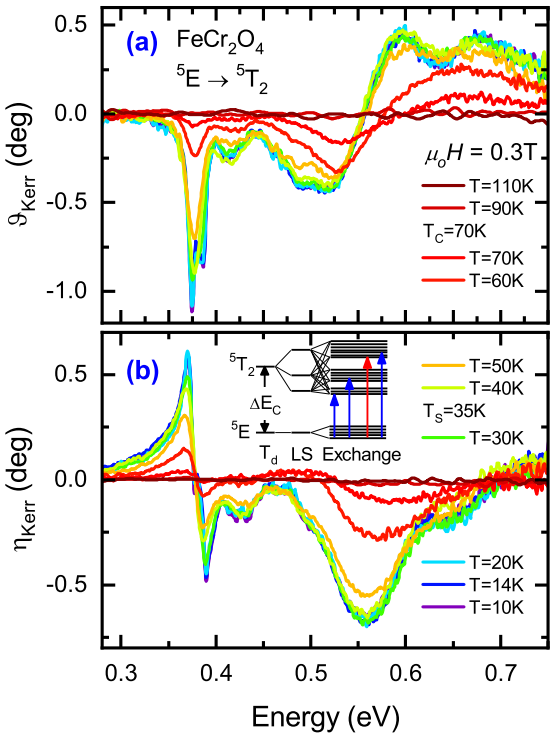

FIG. 2. Temperature dependence of the complex magneto-optical Kerr rotation spectra of $FeCr_2O_4$ measured in the mid- and near-infrared photon energy region. Correspondingly to Fig. 1, the magneto-optical Kerr rotation (a) and ellipticity (b) were measured in $\mu_o H = \pm 0.3$ T magnetic field. Similarly to $CoCr_2O_4$, the largest Kerr rotation signal appears at the low-energy side of the $^5E \rightarrow {}^5T_2$ transition of the Fe^{2+} ion. Splitting of the Fe $3d$ orbitals is schematically reproduced from Refs. [14,33] in the same way as in Fig. 1.

rotation spectra at the low-energy sides of each d-d transition of both materials. The low-energy-side peak of the Co^{2+} ions located at about 0.78 eV reaches a value of $\vartheta_{Kerr} = 12^\circ$ at $T = 10$ K. This excitation exhibits a similarly strong ellipticity signal with a dispersive line shape. For further analysis of the spectral features, off-diagonal optical conductivity spectra were calculated according to Eq. (1).

B. Diagonal and off-diagonal optical conductivity spectra

Figures 3 and 4 show the off-diagonal optical conductivity spectra along with the real part of the diagonal optical conductivity for $CoCr_2O_4$ and $FeCr_2O_4$, respectively. The diagonal optical conductivity spectrum sums up the contributions from transitions excited by right and left ($\Delta J_z = \pm 1$) circularly polarized photons as well as noncircular contributions ($\Delta J_z = 0$). In contrast, the off-diagonal optical conductivity corresponds to the difference between the contributions coming from left and right circularly polarized photons, hence it can have both positive or negative signs.

The temperature dependence of the off-diagonal optical conductivity has a similar evolution for both compounds. Below T_C, the magnitude of the signal gradually increases with decreasing temperature and saturates at about 30 K, roughly following the temperature dependence of the magnetization [14,28,34]. The lifetime of the excited states also increases toward lower temperatures, as clearly manifested in the decrease of the linewidths in both the diagonal and off-diagonal conductivity spectra.

In $CoCr_2O_4$, there are two bands of excitations centered around 0.8 and 2 eV, which are assigned, respectively, to the $e^4t_2^3\,{}^4A_2 \rightarrow e^3t_2^4\,{}^4T_2$ and $e^4t_2^3\,{}^4A_2 \rightarrow e^3t_2^4\,{}^4T_1$ on-site electronic transitions [35] of the Co^{2+} ions with tetrahedral coordination. Here we note that although the low-energy ${}^4A_2 \rightarrow {}^4T_2$ transition is electric-dipole-forbidden (as $A_2 \otimes T_2 = T_1$ does not contain the T_2 irreducible representation, which is connected to the electric-dipole-allowed transitions), the spin-orbit coupling eventually causes the transition to become electric-dipole-allowed. This is because the SOI splits both the ${}^4T_1$ and ${}^4T_2$ multiplets to the same electronic states. As a further demonstration, the spectral weight in the diagonal spectra [$\propto \int_{\omega_{min}}^{\omega_{max}} \sigma_{xx}(\omega)d\omega$] of the ${}^4A_2 \rightarrow {}^4T_2$ transition allowed by SOI is smaller by a factor of 5 than that of the ${}^4A_2 \rightarrow {}^4T_1$ band. In addition to their different magnitudes, there is a sign difference between the off-diagonal conductivity of the two d-d bands as it has been predicted for the irreducible representations of the different excited (${}^4T_1$ and ${}^4T_2$) states in the framework of the crystal-field theory [33].

In $FeCr_2O_4$, similarly to $FeCr_2S_4$, a single branch of excitation is centered at about 0.4 eV [21]. This excitation has been assigned to the $e^3t_2^3\,{}^5E \rightarrow e^2t_2^4\,{}^5T_2$ transitions of the tetrahedrally coordinated Fe^{2+} ions.

C. Temperature dependence of the magneto-optical effect

Figure 5 shows the strength of the magneto-optical effect in $FeCr_2O_4$ and $CoCr_2O_4$ as a function of temperature, represented by integrals of the real and imaginary parts of the optical conductivity spectra over the spectral window of our study. Since the off-diagonal conductivity changes sign throughout the spectral range, the absolute value of its real and imaginary parts was integrated [$\int |\sigma_{xy}(E)|dE$] as an overall measure of the magneto-optical effect in the two compounds. For comparison, the temperature dependence of the magnetization is also plotted in the two cases. The magneto-optical effect emerges below the magnetic ordering temperature and it grows roughly as the magnetization, though considerable deviations between them are discerned well below T_C. This may come from the fact that the magneto-optical signal in our case specifically probes one component of the local magnetization of the Co or Fe ions, while the overall magnetization has contributions from the Cr ions as well. The nonmonotonous behavior of the magnetization implies different temperature dependences of the A and Cr sublattice magnetizations. On the other hand, the magneto-optical signal, which measures the sublattice magnetization of the A ions, increases monotonously below T_C.

We note that the onset of magnetic ordering is different when probed via the magnetization and magneto-optical measurements. In fact, this difference originates from the sample quality, namely the high sensitivity of T_C to oxygen stoichiometry [14,36,37]. The overall stoichiometry can be slightly different for the two samples used for the magnetization and the magneto-optical studies. However, it is perhaps more important that the magnetization measurement probes the bulk of the crystal, while the magneto-optical detection is limited to a

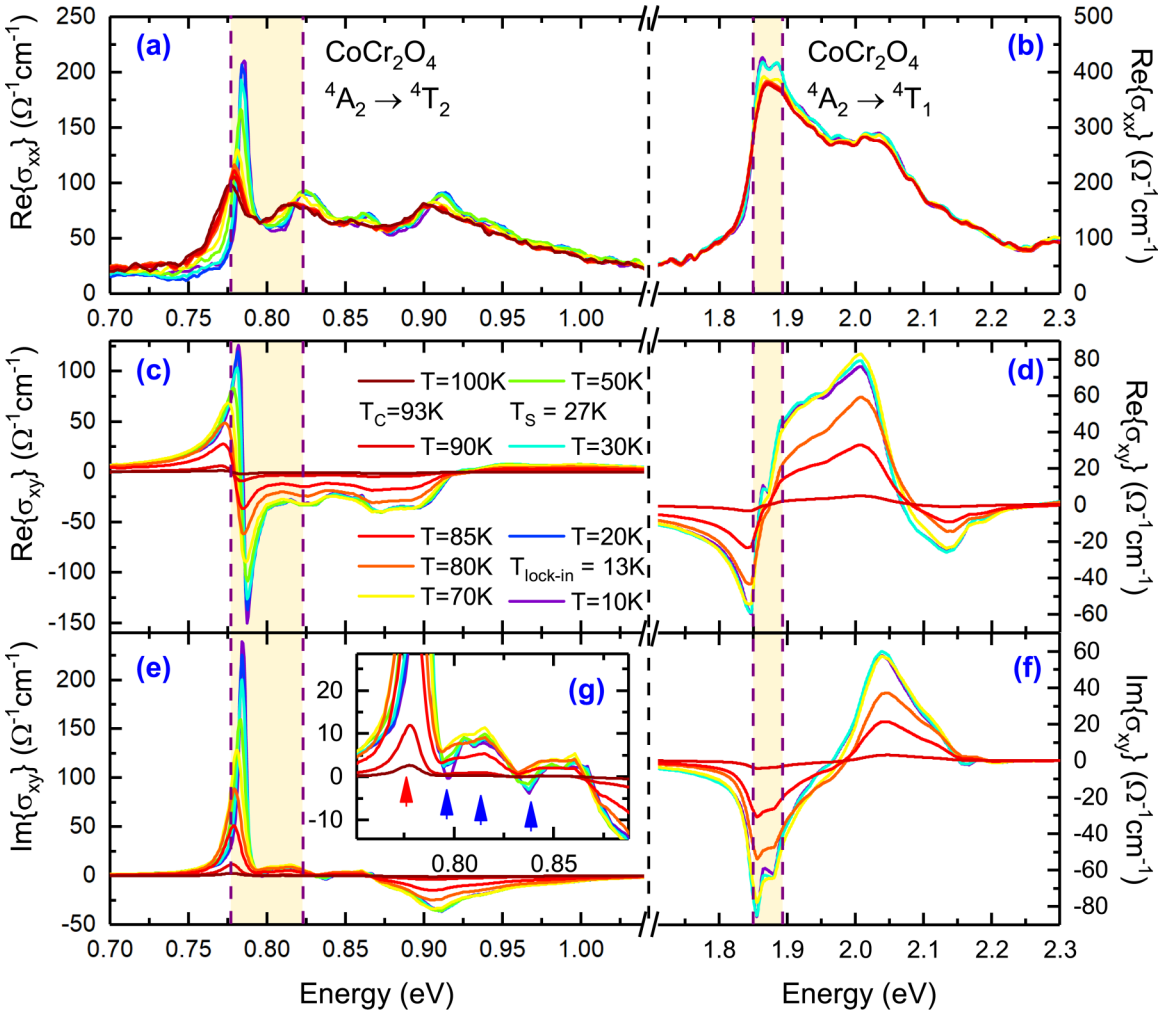

FIG. 3. Diagonal (a),(b) and complex off-diagonal (b)–(f) optical conductivity spectra at various temperatures of the two transitions of $CoCr_2O_4$. Regions of the electronic states approximated by the free-ion spin-orbit splitting for the $^4T_2$ and $^4T_1$ multiplets are indicated by the colored stripes around 0.8 and 1.9 eV, respectively. Blue and red arrows indicate the possible arrangement of the SOI and Zeeman split ZPLs for the $^4T_2$ multiplet.

submicrometer penetration depth below the as-grown surface. Therefore, the different transition temperatures observed in the two cases may also represent the T_C values characteristic of the bulk and the surface, with different oxygen stoichiometry.

D. Fine structure of the *d-d* transitions

We turn now to a discussion of the fine structure describing both the diagonal and off-diagonal optical conductivity spectra in comparison with the results reported for compounds substitutionally doped with Co^{2+} or Fe^{2+} in tetrahedral or octahedral sites [38–45]. In general, there are sharp, distinct features emerging at the low-energy sides of each band, with a significant temperature dependence. This sharp and well-separated feature is the most prominent one for the low-energy side of the T_2 multiplet of $CoCr_2O_4$, and it was also discerned in the temperature dependence of both σ_{xx} and σ_{xy} in Fig. 3. At the higher-energy side of these multiplets, there are additional transitions with a much larger linewidth and a less significant temperature dependence. Usually, the parallel analysis of the diagonal and off-diagonal spectra supports an unambiguous assignment of optical excitations. While the diagonal spectra contain the sum of all transitions, namely $\Delta J_z = 0$ and $\Delta J_z \pm 1$ transitions, the off-diagonal spectra contain only the $\Delta J_z \pm 1$ transitions with different signs. However, the fine structure of the *d-d* bands due to the strong overlap between these broad transitions does not allow a precise assignment of the excitations.

The widths of the *d-d* bands are $\delta E \approx 0.3$ and ≈ 0.5 eV for the $^4A_2 \rightarrow {}^4T_2$ and $^4A_2 \rightarrow {}^4T_1$ transitions of the Co^{2+} ion, respectively, and $\delta E \approx 0.4$ eV for the $^5E \rightarrow {}^5T_2$ transitions of the Fe^{2+} ion. On the other hand, the bandwidths reported for the *d-d* transitions of Co^{2+} and Fe^{2+} ions [14,38,41,42,44,45] in general are in the range of $\delta E \approx 0.1-0.3$ eV. The observed large bandwidths cannot be explained exclusively by the effect of first-order spin-orbit coupling, since the free ion spin-orbit interaction parameters are only $\zeta_o = 410$ cm$^{-1} \approx 50$ meV for the $^5T_2$ multiplet of Fe^{2+} and $\zeta_o = 533$ cm$^{-1} \approx 70$ meV for both the $^4T_1$ and $^4T_2$ multiplets of Co^{2+}. Moreover, the strength of the SOI should be further reduced in crystals due to hybridization with the ligand orbitals [14,33,46,47]. The hypothetical broadening of the *d-d* bands, which would

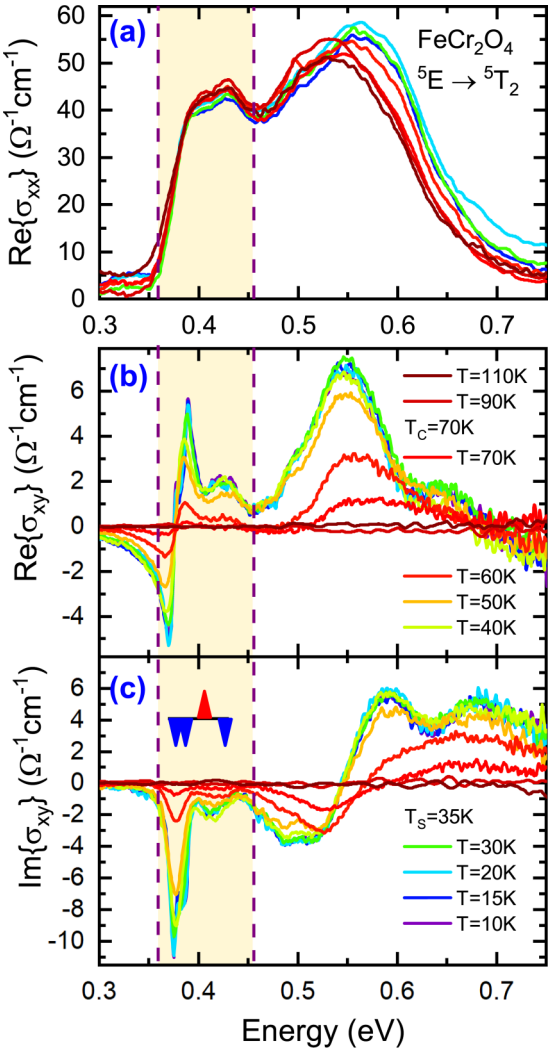

FIG. 4. Temperature dependence of the diagonal (a) and the complex off-diagonal (b,c) optical conductivity spectra of $FeCr_2O_4$. The approximated region of the electronic states of the free-ion spin-orbit-split $^5T_2$ multiplet is indicated by the colored stripes. Arrows within the region mark the possible assignment for SOI-split ZPL transitions, while the outside region corresponds to the phonon sidebands.

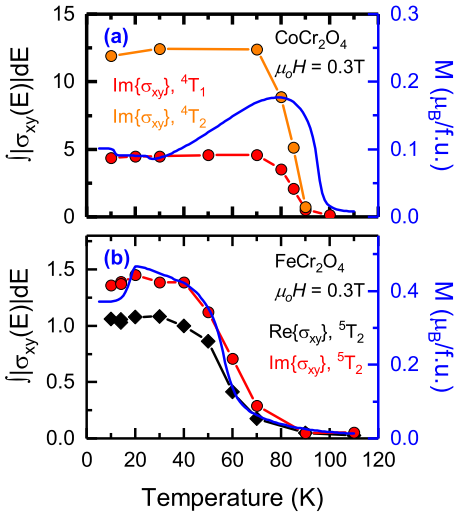

FIG. 5. Temperature dependence of the magneto-optical effect compared to the magnetization of $CoCr_2O_4$ (a) and $FeCr_2O_4$ (b). The strength of the magneto-optical effect is represented by the integrals of the absolute values of the real and imaginary parts of the off-diagonal conductivity over the spectral window of the measurement. Magnetization was measured in a $\mu_o H = 0.3$ T magnetic field along the [001] axis of the crystal.

correspond to the free-ion spin-orbit interaction parameters, is indicated in Figs. 3 and 4 by the highlighted yellow regions.

In dilute systems with few tetrahedrally coordinated A^{2+} ions, the increased bandwidth is explained by two main factors: (i) the second-order spin-orbit interaction, which causes a slight additional split of the orbital degeneracy of the d states [41], and (ii) the emergence of phonon sidebands at the high-energy side of the zero phonon d-d multiplets due to the dynamic Jahn-Teller effect [38,39,41–45,48]. The dynamic Jahn-Teller effect is an interplay between the purely orbital excitations of an ion [zero-phonon line (ZPL)] and the vibrational modes of the surrounding lattice. Due to the hybridization of these excitations, part of the spectral weight is transferred from the ZPL to the phonon sidebands (see Fig. 6). In most dilute systems, multiplets of the A^{2+} ion are mostly coupled to phonon modes with one-dimensional representation (typically to the A_1 breathing mode of the ligand cage). The normalized intensity of the nth sideband is well described by a Poisson distribution [49]:

$$I_n = e^{-S}\frac{S^n}{n!}, \tag{2}$$

where $S = \frac{E_R}{\hbar\omega}$ is the strength of the electron-phonon coupling, E_R is the energy shift of the highest intensity sideband, $\hbar\omega$ is the energy of the coupled phonon mode, and $I_0 = e^{-S}$ is the intensity of the ZPL. The expectation number of the phonons coupled to the electronic excitation is equal to the strength of the coupling ($S = \langle n \rangle$). Therefore, in dilute systems, the local vibrations of the ligands surrounding the A^{2+} ions give sharp phonon sidebands to the optical spectra, which is schematically illustrated in Fig. 6(b).

In high-symmetry crystals with a regular network of A^{2+} ions, several different phonons with a higher-dimensional representation may couple to the electronic excitations. In this case, Eq. (2) is expanded to multidimensional form and the phonon sidebands are widened [49–52], which is illustrated in Fig. 6(c). Here we note that the intensity of the ZPL depends on the S coupling constant. For $S = 1$, the ZPL is the strongest and the phonon sidebands are evanescent, while for large coupling the ZPL is negligible and the phonon sidebands dominate the spectrum.

The strength of the electron-phonon coupling in spinel compounds can be estimated by determining E_R and $\hbar\omega$ separately. $E_R \approx 0.15$ eV is well approximated by the width of the multiplets ($2E_R = \delta E \approx 0.3$ eV), which is generally appropriate for both oxide and chalcogenide spinels [14]. The phonon energy of the coupled modes can be estimated by the highest-energy optical phonon mode, as it is mainly composed of lattice vibrations of the lighter ligand nuclei. Therefore, for oxide spinels the highest-energy optical phonon modes ($\hbar\omega \approx 74$ meV) bring a relatively small coupling constant

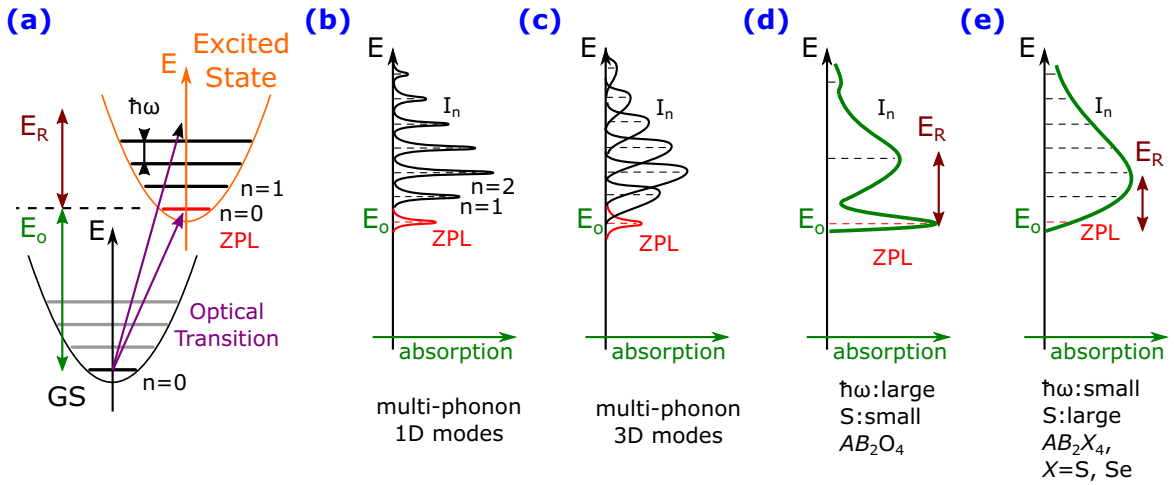

FIG. 6. (a) Schematic illustration of the hybrid electron-lattice excitations in the presence of electron-phonon coupling. Transitions are allowed from the ground state to the phonon sidebands of the excited multiplet, which increases the spectral width of the transition. (b)–(e) Illustration of the absorption spectra for different models: (b) Dilute systems have a spiky spectrum, while (c) regular crystals have wider phonon sidebands. In oxide spinels, the $\hbar\omega$ phonon energy is larger and the S coupling parameter [Eq. (2)] is smaller as compared to chalcogenide spinels. Therefore, in the former case, shown in panel (d), the ZPL is less overlapped by the phonon sidebands, while in the second case, sketched in panel (e), the phonon sidebands are not just more overlapped with the ZPL, but also most of the intensity is transferred to the sidebands.

($S = 2$) [22]. On the other hand, in sulfur- and selenium-based spinels the ligands are heavier ($\hbar\omega \approx 49$ and ≈ 37 meV, respectively [53]) and the electron-phonon couplings are also higher, $S = 3$ and 4, respectively. In sulfide and selenide spinels, the expansive $3p$ and $4p$ orbitals of the ligand ions have stronger hybridization with the $3d$ orbitals of the A^{2+} transition metal ions, thus stronger electron-phonon coupling is expected, in agreement with the observations.

E. Criteria of strong magneto-optical effects

Based on our experimental results, we list the criteria of strong magneto-optical effects at on-site d-d transitions of transition metal ions in magnetic crystals. In addition to the well-known criteria (i)–(v), we add two empirical and material-specific ones:

(i) To make the on-site d-d transitions electric-dipole-allowed, the inversion symmetry at the transition metal sites needs to be broken, e.g., by the tetrahedral coordination of the sites.

(ii) Since spin-forbidden transitions are usually weak, the on-site d-d transitions have to be spin allowed as well. This excludes the ions with a half-filled d shell carrying spin $S = 5/2$.

(iii) The material has to be a semiconductor with a sufficiently large gap so that the d-d transitions lie within the optical band gap.

(iv) Strong spin-orbit interaction is needed to split the degeneracy of the d orbitals within the crystal-field multiplets (e and t_2 states in spinels with cubic symmetry).

(v) The material has to be either a ferro- or ferrimagnet, where the magnetic exchange interaction removes the degeneracy of the states with different J_z values.

(vi) Among the SOI-split multiplets of the excited states, there should be only one with a higher spin degeneracy than the ground state. In this case, the sum of the oscillator strengths of the remaining transitions to the $|J_z| - 1$ excited states will have the same contribution to the magnetocircular birefringence as the single transition to the $|J_z| + 1$ state.

(vii) The ligand ions should be light, so the $\hbar\omega$ is high and the phonon sidebands are well separated from the ZPL. Furthermore, hybridization between the orbitals of the transition metal and the ligand ions should be small. The electron-phonon coupling should be weak, therefore only a small part of the oscillator strength is transferred to the phonon sidebands.

By a systematic analysis of the Tanabe-Sugano diagrams [33], and taking into account the effect of spin-orbit coupling, we found a few transition metal ions with a tetrahedral environment that might be in compliance with these conditions. In addition to the interesting $e^4t_2^3\ {}^4A_2$ ground- and $e^3t_2^4\ {}^4T_2$ excited-state combination of Co^{2+}, the V^{3+} ion has a similarly favorable electron configuration. Experimental studies on vanadium-doped compounds have shown that tetrahedrally coordinated V^{3+} ions usually realize $e^2\ {}^3A_2$ ground and $e^1t_2^1\ {}^3T_1$ excited states, which could be optimal for strong magneto-optical effects [43,54]. However, V^{3+} ions, similarly to the Cr^{3+} ions, dominantly occupy octahedral environments when forming a regular sublattice in crystals and only enter tetrahedral sites as dopants [54,55]. Thus, they are unfavored by condition (i). Tetrahedrally coordinated Mn^{+2} ions carry $S = 5/2$ spins, hence a strong magneto-optical response from these ions is excluded by condition (ii). Optical excitations of Fe^{2+} ions in tetrahedral coordination do not fulfill condition (vi) as observed in former works [14,21,22,41,42,44,45] as well as in the present study. Tetrahedrally coordinated Ni^{2+} and Cu^{2+} ions show orbital degeneracy, which is lifted by the distortion of oxygen tetrahedra upon the cooperative Jahn-Teller transition [56–58]. In the distorted state, for both ions there is no orbital degeneracy either in the ground or the excited states. Correspondingly, we expect a weak magneto-optical response for these ions. Therefore, the best candidates that can generate strong magneto-optical effects are the tetrahedrally coordinated Co^{2+} ions.

IV. CONCLUSIONS

We observed a strong magneto-optical Kerr effect at the on-site d-d transitions of Co^{2+} and Fe^{2+} ions in the spinel oxides $CoCr_2O_4$ and $FeCr_2O_4$. The magneto-optical Kerr rotation $\vartheta_{\mathrm{Kerr}} = 12^{\circ}$ observed in $CoCr_2O_4$ is the largest reported so far in magnetic semiconductors and insulators. We discussed the criteria of strong magneto-optical effects in insulating transition metal oxide compounds and the unique potential of the tetrahedrally coordinated Co^{2+} ions.

ACKNOWLEDGMENTS

The authors are grateful to N. Nagaosa, T. Arima, and K. Penc for fruitful discussions, and Á. Butykai for the technical support in magnetization measurements. This work was supported by the Hungarian Research Funds OTKA K 108918, OTKA PD 111756, National Research, Development and Innovation Office – NKFIH, ANN 122879, and Bolyai 00565/14/11 and by the Deutsche Forschungsgemeinschaft through the Transregional Collaborative Research Center TRR 80.

[1] M. A. Butler, S. J. Martin, and R. J. Baughman, Appl. Phys. Lett. **49**, 1053 (1986).
[2] Y. Hwang, H. Kim, S. Cho, and Y. Um, J. Appl. Phys. **100**, 063509 (2006).
[3] V. I. Belotelov, I. A. Akimov, M. Pohl, V. A. Kotov, S. Kasture, A. S. Vengurlekar, A. V. Gopal, D. R. Yakovlev, A. K. Zvezdin, and M. Bayer, Nat. Nanotechnol. **6**, 370 (2011).
[4] H. Ebert and G. Schutz, *Spin-Orbit-Influenced Spectroscopies of Magnetic Solids* (Springer-Verlag, Berlin, 1996).
[5] S. Sugano and N. Kojima, *Magneto-Optics* (Springer-Verlag, Berlin, 1999).
[6] H. Shimizu, M. Miyamura, and M. Tanaka, Appl. Phys. Lett. **78**, 1523 (2001).
[7] R. B. Versteeg, I. Vergara, S. D. Schäfer, D. Bischoff, A. Aqeel, T. T. M. Palstra, M. Grüninger, and P. H. M. van Loosdrecht, Phys. Rev. B **94**, 094409 (2016).
[8] N. J. Laurita, G. G. Marcus, B. A. Trump, J. Kindervater, M. B. Stone, T. M. McQueen, C. L. Broholm, and N. P. Armitage, Phys. Rev. B **95**, 235155 (2017).
[9] H. Feil and C. Haas, Phys. Rev. Lett. **58**, 65 (1987).
[10] S. Bordács, I. Kézsmárki, K. Ohgushi, and Y. Tokura, New J. Phys. **12**, 053039 (2010).
[11] R. Pittini, J. Schoenes, O. Vogt, and P. Wachter, Phys. Rev. Lett. **77**, 944 (1996).
[12] W. Reim, J. Schoenes, F. Hulliger, and O. Vogt, J. Magn. Magn. Mater. **54–57**, 1401 (1986).
[13] V. N. Gridnev, B. B. Krichevtsov, V. V. Pavlov, and R. V. Pisarev, J. Exp. Theor. Phys. **65**, 68 (1997).
[14] K. Ohgushi, Y. Okimoto, T. Ogasawara, S. Miyasaka, and Y. Tokura, J. Phys. Soc. Jpn. **77**, 034713 (2008).
[15] M. N. Popova, E. P. Chukalina, T. N. Stanislavchuk, B. Z. Malkin, A. R. Zakirov, E. Antic-Fidancev, E. A. Popova, L. N. Bezmaternykh, and V. L. Temerov, Phys. Rev. B **75**, 224435 (2007).
[16] E. A. Popova, N. I. Leonyuk, M. N. Popova, E. P. Chukalina, K. N. Boldyrev, N. Tristan, R. Klingeler, and B. Büchner, Phys. Rev. B **76**, 054446 (2007).
[17] B. Bleaney and K. W. H. Stevens, Rep. Prog. Phys. **16**, 108 (1953).
[18] K. D. Bowers and J. Owen, Rep. Prog. Phys. **18**, 304 (1955).
[19] J. Hemberger, P. Lunkenheimer, R. Fichtl, H.-A. K. von Nidda, V. Tsurkan, and A. Loidl, Nature (London) **434**, 364 (2005).
[20] S. Weber, P. Lunkenheimer, R. Fichtl, J. Hemberger, V. Tsurkan, and A. Loidl, Phys. Rev. Lett. **96**, 157202 (2006).
[21] K. Ohgushi, T. Ogasawara, Y. Okimoto, S. Miyasaka, and Y. Tokura, Phys. Rev. B **72**, 155114 (2005).
[22] V. Kocsis, S. Bordács, D. Varjas, K. Penc, A. Abouelsayed, C. A. Kuntscher, K. Ohgushi, Y. Tokura, and I. Kézsmárki, Phys. Rev. B **87**, 064416 (2013).
[23] N. Menyuk, K. Dwight, and A. World, J. Phys. (Paris) **25**, 528 (1964).
[24] G. Lawes, B. Melot, K. Page, C. Ederer, M. A. Hayward, T. Proffen, and R. Seshadri, Phys. Rev. B **74**, 024413 (2006).
[25] M. Tanaka, T. Tokoro, and Y. Aiyama, J. Phys. Soc. Jpn. **21**, 262 (1966).
[26] K. Tsuda, D. Morikawa, Y. Watanabe, S. Ohtani, and T. Arima, Phys. Rev. B **81**, 180102(R) (2010).
[27] K. Tomiyasu, J. Fukunaga, and H. Suzuki, Phys. Rev. B **70**, 214434 (2004).
[28] G. Shirane, D. E. Cox, and S. J. Pickart, J. Appl. Phys. **35**, 954 (1964).
[29] H. Ishibashi and T. Yasumi, J. Magn. Magn. Mater. **310**, e610 (2007).
[30] K. Sato, Jpn. J. Appl. Phys. **20**, 2403 (1981).
[31] L. Demkó, G. A. H. Schober, V. Kocsis, M. S. Bahramy, H. Murakawa, J. S. Lee, I. Kézsmárki, R. Arita, N. Nagaosa, and Y. Tokura, Phys. Rev. Lett. **109**, 167401 (2012).
[32] V. Antonov, B. Harmon, and A. Yaresko, *Electronic Structure and Magneto-optical Properties of Solids* (Kluwer Academic, Dordrecht, 2004).
[33] S. Sugano, Y. Tanabe, and H. Kamimura, *Multiplets of Transition-Metal Ions in Crystals* (Academic Press, New York, 1970).
[34] Y. Yamasaki, S. Miyasaka, Y. Kaneko, J.-P. He, T. Arima, and Y. Tokura, Phys. Rev. Lett. **96**, 207204 (2006).
[35] The $e^n t_2^m {}^S\Gamma$ notation means that the Γ irreducible representation of a transition metal multiplet, which has S spin degeneracy and the orbital part, is derived from the product of ne and mt_2 crystal-field-split orbitals. In the text, the electron configuration will be omitted for simplicity.
[36] P. Zhang, F. Su, S. Zhang, H. Mei, C. Zhang, X. Luo, J. Dai, and L. Pi, Opt. Express **23**, 17805 (2015).
[37] I. Efthimiopoulos, Z. T. Y. Liu, S. V. Khare, P. Sarin, T. Lochbiler, V. Tsurkan, A. Loidl, D. Popov, and Y. Wang, Phys. Rev. B **92**, 064108 (2015).
[38] R. Pappalardo and R. E. Dietz, Phys. Rev. **123**, 1188 (1961).
[39] A. D. Liehr and C. J. Ballhausen, J. Mol. Spectrosc. **2**, 342 (1958).
[40] C. H. Henry, S. E. Schnatterly, and C. P. Slichter, Phys. Rev. **137**, A583 (1965).

[41] G. A. Slack, F. S. Ham, and R. M. Cherenko, Phys. Rev. **152**, 376 (1966).
[42] S. Wittekoek, R. P. van Stapele, and A. W. J. Wijma, Phys. Rev. B **7**, 1667 (1973).
[43] P. Koidl, O. F. Schirme, and U. Kaufmann, Phys. Rev. B **8**, 4926 (1973).
[44] A. Hjortsberg, B. Nygren, J. Vallin, and F. S. Ham, Phys. Rev. Lett. **39**, 1233 (1977).
[45] A. Hjortsberg, J. T. Vallin, and F. S. Ham, Phys. Rev. B **37**, 3196 (1988).
[46] C. K. Jorgensen, *Absorption Spectra and Chemical Bonding in Complexes* (Elsevier, Amsterdam, 2013).
[47] R. G. Burns, *Mineralogical Applications of Crystal Field Theory* (Cambridge University Press, Cambridge, UK, 1970).
[48] Y. Toyozawa and M. Inoue, J. Phys. Soc. Jpn. **21**, 1663 (1966).
[49] Y. Toyozawa, *Optical Processes In Solids* (Cambridge University Press, Cambridge, 2003).
[50] R. Kubo and Y. Toyozawa, Prog. Theor. Phys. **13**, 160 (1955).
[51] K. Huang, Proc. R. Soc. London, Ser. A **208**, 352 (1951).
[52] M. Lax, J. Chem. Phys. **20**, 1752 (1952).
[53] T. Rudolf, Ch. Kant, F. Mayr, J. Hemberger, V. Tsurkan, and A. Loidl, New J. Phys. **9**, 76 (2007).
[54] S. Kück and P. Jander, Opt. Mater. **13**, 299 (1999).
[55] D. T. Sviridov and R. K. Sviridova, J. Appl. Spectrosc. **34**, 431 (1981).
[56] K. Siratori, J. Phys. Soc. Jpn. **23**, 948 (1967).
[57] O. Crottaz, F. Kubel, and H. Schmid, J. Mater. Chem. **7**, 143 (1997).
[58] B. J. Kennedy and Q. Zhou, J. Solid State Chem. **181**, 2227 (2008).